Effect of Temperature on the Transport of Water and Neutral Solutes across Nanofiltration Membranes

ARTICLE *in* LANGMUIR · APRIL 2007

Impact Factor: 4.46 · DOI: 10.1021/la060268p · Source: PubMed

4 AUTHORS, INCLUDING:

Nihel Ben Amar
National Institute of Applied Sciences and Te…

29 PUBLICATIONS **269** CITATIONS

Articles

Effect of Temperature on the Transport of Water and Neutral Solutes across Nanofiltration Membranes

N. Ben Amar,[†,‡] H. Saidani,[†,‡] A. Deratani,[‡] and J. Palmeri*[,‡]

Laboratoire de Modélisation Mathématique et Numérique dans les Sciences de l'Ingénieur, ENIT, Campus Universitaire, B.P 37 Le belvédère 1002, Tunis, Tunisia, and Institut Européen des Membranes, cc047, UMR5635 CNRS-ENSCM-Université Montpellier II, 2 Place Eugène Bataillon, 34095 Montpellier Cedex 5, France

Received January 27, 2006. In Final Form: December 22, 2006

We carry out a detailed experimental and theoretical study of the influence of temperature on nanofiltration performance using the Desal5DK membrane. Experimental results for the permeate volume flux density and rejection of four neutral solutes (glycerin, arabinose, glucose, and sucrose) are presented for temperatures between 22 and 50 °C. Solute rejection is modeled using a hindered transport theory that allows us to unveil the crucial role played by changes in the membrane structural parameters (effective pore radius and membrane thickness) due to changes in temperature.

Introduction

Besides important uses in the desalination of geothermal brackish water (2−4 g/L, 50 to 55 °C), nanofiltration (NF) membranes also have a large number of other industrial applications (paper, sugar, food, textile, etc.) in which the temperature can be high and may even reach 90 °C (bleaching and dyeing applications). Moreover, nanofiltration may be used in hybrid systems for seawater desalination coupled with thermal desalination processes, such as NF−MSF (multistage flash)[1] and NF−MSF−RO (reverse osmosis).[2] It is also used, for example, as the final stage in the Mery-sur-Oise river water treatment plant to make drinking water.[3,4] In these surface water applications, the temperature of the feed (sea or river water) varies with the season, and it has been observed that the temperature plays a significant role on nanofiltration membrane performance. For a better mastery of all the applications described above, it is essential to obtain a detailed understanding of the influence of temperature on nanofiltration performance (permeate volume flux density and solute rejection). In spite of the increasingly widespread industrial use of NF and RO membranes, much remains to be learned about the physicochemical mechanisms governing solvent and solute transport at the molecular level. The acquisition of such knowledge, which depends on simultaneous advances in preparation and modeling methods, would have a potentially large payoff in terms of the elaboration of cost-effective tailor-made nanoporous membranes for specific industrial applications (such as low-cost seawater desalination).

Membrane manufacturers have only treated the effect of temperature on water flux and give in their product literature correlations which correct the water flux compared to that given at a reference temperature (20 or 25 °C).[5] In this way, plant operators can estimate the conversion factor corresponding to the real feed temperature.

The effect of temperature on flux and rejection of solutes (neutral and charged) has already been touched upon in the areas of microfiltration (MF), ultrafiltration (UF), nanofiltration (NF), and reverse osmosis (RO). Perhaps the earliest investigation of temperature effects was a study of the sodium chloride−water−cellulose acetate system.[6] More recent work can be found in studies of MF,[7] UF,[8] NF,[3,4,9−11] and RO.[12,13]

All of the above-mentioned studies show an increase of permeate volume flux with increasing temperature. There are, however, variable results for solute rejection. Although the usual trend for NF is a decrease in rejection with increasing temperature, Schaep et al.[11] find an increase of the rejection of divalent ions

* Corresponding author. Current address: Laboratoire de Physique Théorique, IRSAMC UMR CNRS-UPS 5152, Université Paul Sabatier, 118 route de Narbonne, 31062 Toulouse CEDEX 4, France. Tel: +33 (0)5.61.55.61.77. Fax: +33 (0)5.61.55.60.65. E-mail: john.palmeri@irsamc.ups-tlse.fr.

† ENIT.

‡ CNRS.

(1) Al-Sofi, M. A. K.; Hassan, A. M.; Mustafa, G. M.; Dalvi, A. G. I.; Kither, M. N. M. *Desalination* **1998** *118*, 123−129.

(2) Hassan, A. M.; Al-Sofi, M. A. K.; AL-Amoudi, A. S.; Jamaluddin, A. T. M.; Farooque, A. M.; Rowaili, A.; Dalvi, A. G. I.; Kither, N. M.; Mustafa, G. M.; Al- Tisan, I. A. R. *Desalination* **1998**, *118*, 35−51.

(3) Wittman, E. La Nanofiltration dans le domaine du traitement des eaux: conditions d'application et modélisation. Ph.D. Thesis, University of Montpellier II, France, 1998.

(4) Ventresque, C.; Gisclon, V.; Bablon, G.; Chagneau, G. *Desalination* **2000**, *131*, 1−16.

(5) Desal Pure Water, Membrane Technology & Applications; GE-Osmonics; 2003.

(6) Londsdale, H. K.; Merten, U.; Riley, R. L. *J. Appl. Polym. Sci.* **1965**, *9*, 1341.

(7) Mohammadi, T.; Pak, A.; Karbassian, M.; Golshan, M. *Desalination* **2004**, *168*, 201−205.

(8) Huisman, I. H.; Dutré, B.; Persson, K. M.; Trägardh, G. *Desalination* **1997**, *113*, 95−103.

(9) Tsuru, T.; Izumi, S.; Yoshiota, T.; Asaeda, M. *AIChE J.* **2000**, *46*, 565−574.

(10) Sharma, R. R.; Agrawal, R.; Chellam, S. *J. Membr. Sci.* **2003**, *223*, 69−87.

(11) Schaep, J.; Van der Bruggen, B.; Uytterhoeven, S.; Croux, R.; Vandecasteele, C.; Wilms, D.; Van Houtte, E.; Vanlerberghe, F. *Desalination* **1998**, *119*, 295−302.

(12) Goosen, M. F. A.; Sablani, S. S.; Al-Maskari, S. S.; Albelushi, R. H.; Wilf, M. *Desalination* **2002**, *144*, 367−372.

(13) Kilduff, J. E.; Mattaraj, S.; Wigton, A.; M. Kitis, M.; Karanfil, T. *Water Res.* **2004**, *38*, 1026−1036.

10.1021/la060268p CCC: $37.00
Published on Web 02/17/2007

with temperature, and Mänttäri et al.[14] find that the salt rejection is temperature-independent. These studies were carried out with different nanofiltration membranes (UTC20 in ref 10 and NF200, Desal5 DK, and NF200 in ref 14), but at the same transmembrane pressure (10 bar).

The increase of the water flux with increasing temperature is usually attributed (see, for example, ref 11) to an amelioration of the viscous transport via a decrease in the intramembrane solution viscosity, usually considered to be correlated with that of bulk water. There is evidence, however, that the decrease in bulk solution viscosity alone cannot completely explain the increase in water flux, leading to the suggestion that the pure water transport in nanopores is an activated permeation process.[10] In ref 14, it has been shown that, when the temperature increases, the glucose solution (250 ppm) flux increases for different membranes (Desal5DL (Osmonics), XN-40 (Trisep), and TS-80 (Trisep)). It has also been noted that the measured solution flux obtained with the Desal5DL membrane is perfectly reversible when the temperature is decreased, which is not the case for the other membranes studied. This increase of water permeation with temperature may be linked in part to the expansion of the polymeric membrane structure at high temperatures. The irreversibility of membrane performance may be due to the permanent reorientation of the polymer chains in looser membranes (with polymer structures that are less dense when compared to tighter membranes[15]).

The effect of temperature on water flux and its relation to the bulk water viscosity was also studied in ref 9 using three homemade inorganic membranes. It was found that for these membranes the increase in water permeation cannot be attributed solely to the temperature dependence of the bulk viscosity. Since inorganic membrane structure is expected to be thermally stable, it was suggested that this discrepancy could be due to factors other than the temperature-dependent structural changes usually evoked for organic membranes. Several alternative explanations were given: (1) water permeation may be an activated process, (2) the adsorption of water on the pore walls may reduce the effective pore diameter (the thickness of the adsorbed layer would decrease with increasing temperature, making the pore diameter larger), and finally (3) the viscosity considered is usually the bulk viscosity, which may be different from the viscosity in the pores; indeed, the intrapore viscosity may have a stronger dependence on temperature than the bulk one.

The temperature dependence of neutral solute rejection was studied in ref 10, and it was found that with the Desal5DL membrane, for example, the rejection was independent of permeate flux at all temperatures for the extreme solute sizes, namely, the highest molecular weight solutes, such as sucrose and raffinose, and the lowest molecular weight solute, ethanol. For intermediate molecular weight solutes (ethylene glycol, glycerin, etc.), it was found that the rejection decreases with increasing temperature. For the Desal5DL membrane at 23 °C, a mean pore radius of 0.3 nm was determined using a log-normal model. A larger pore radius (0.52 nm) was obtained using a hindered transport pore model, and an increase of 21% was noted in the pore radius of the Desal5DL membrane when the temperature increased from 5 to 41 °C. These results are in agreement with those of ref 14 where it was found that for the three membranes studied, including the Desal5DK, the rejection of total dissolved carbon (TDC) in an industrial effluent (mechanical pulp plant) decreased with increasing temperature. The rejection of inorganic salts, however, seemed to be temperature-independent; it was suggested in ref 14 that this result is due to the predominance of the charge, and not size, exclusion mechanism in this case. These results, however, are in contradiction with those of ref 11, which show that salt rejection decreases with increasing temperature. In ref 9, neutral solute rejection was also studied as a function of temperature using inorganic nanofilters, and it was found that, at fixed volume flux density, rejection decreases with increasing temperature. Although the experimental results were interpreted in terms of phenomenological solute permeability and filtration reflection coefficients, no attempt was made to relate these coefficients to membrane structural properties.

Faced with the industrial importance of the problem at hand and the at times contradictory results summarized above, we have carried out a detailed study of the effect of temperature on nanofiltration performance. To avoid complicated electrostatic and dielectric effects, we focus here only on the nanofiltration of neutral solutes and study the temperature dependence of hindered solute transport. For this purpose, permeation and rejection experiments were conducted, and the rejection results were analyzed using the *NanoFlux* computer program[16,17] which is based on the hindered transport theory[18] for neutral solutes. This theory can be used to estimate the changes in the structural parameters of a membrane (effective pore radius and membrane thickness) due to changes in temperature.

The membrane used in this work is the composite Desal5DK membrane (GE-Osmonics), reported to be thermally resistant up to 90 °C when used in flat sheets. In the experiments, a low solute concentration was used (1 g/L) in order to render solute−solute interactions negligible and justify the approximations inherent in the dilute solution transport model we have adopted.

Our general strategy is as follows: By measuring and modeling the pure water permeability and neutral solute rejection, we attempt to isolate that part of the temperature dependence of these quantities that *cannot* be attributed to changes in *intrapore* viscosity or solute diffusivity that follow the temperature dependence of the corresponding bulk quantities. We attribute residual temperature effects, over and beyond those predicted by the temperature dependence of these bulk properties, to hindered transport effects in nanopores and attempt to correlate these effects with temperature variations of the intrinsic structural properties of the membrane, namely, the effective pore radius and membrane thickness. In order to probe the membrane pore radius, r_p, while at the same time limiting the influence of other solute−membrane interactions,[19,20] the model solutes were neutral, their radii, r_s, were relatively large ($0.4 \leq r_s/r_p \leq 0.8$), and their permanent dipole moments were less than 3D (the criterion chosen in ref 20 in order to limit the influence of solute dipole−membrane charge interactions). In such conditions, we believe hindered transport effects to be predominant with other solute−membrane interactions playing only a secondary role (cf. ref 20).

Experimental Section

Setup and Procedure. *Apparatus.* The experimental apparatus (Figure 1) used to study the effect of temperature on flux and rejection

(14) Mänttäri, M.; Pihlajamäki, A.; Kaipainen, E.; Nyström, M. *Desalination* **2002**, *145*, 81−86.

(15) Yao, W. X.; Kennedy, K. J.; Tam, C. M.; Hazlett, J. D. *Can. J. Chem. Eng.* **1994**, *72*, 991−999.

(16) Palmeri, J.; Sandeaux, J.; Sandeaux, R.; Lefebvre, X.; David, P.; Guizard, C.; Amblard, P.; Diaz, J. F.; Lamaze, B. *Desalination* **2002**, *147*, 231−236.

(17) Lefebvre, X.; Palmeri, J.; Sandeaux, J.; Sandeaux, R.; David, P.; Maleyre, B.; Guizard, C.; Amblard, P.; Diaz, J. F; Lamaze, B. *Sep. Purif. Technol.* **2003**, *32*, 117−126.

(18) Deen, W. M. *AIChE J.* **1987**, *33*, 1409−142.

(19) van der Bruggen, B.; Schaep, J.; Wilms, D.; Vandecasteele, C. *J. Membr. Sci.* **1999**, *156*, 29−41.

(20) van der Bruggen, B.; Schaep, J.; Wilms, D.; Vandecasteele, C. *Sep. Sci. Tech.* **2000**, *35*, 169−182.

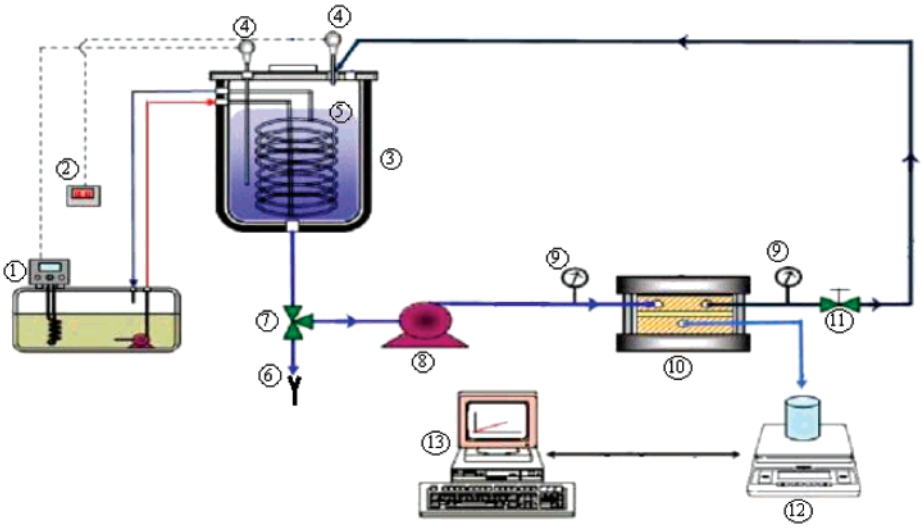

Figure 1. Schematic diagram of the experimental apparatus. 1. circulating thermal bath; 2. bill-poster temperature; 3. feed tank; 4. temperature probe; 5. coil; 6. purge; 7. three-way valve; 8. high-pressure pump; 9. manometer; 10. Sepa CF II cell; 11. pressure control valve; 12. balance; 13. personal computer.

Table 1. Neutral Solute Properties

solute	glycerol	arabinose	glucose	sucrose
molecular weight (kg/kmol)	92	150.13	180	342.3
stokes radii (nm)	0.260	0.323	0.365	0.471
diffusivity ($m^2\ s^{-1}$) at 25 °C	0.94×10^{-9}	0.76×10^{-9}	0.67×10^{-9}	0.52×10^{-9}

Table 2. Characteristics of the Desal5DK Nanofiltration Membrane

rejection	98% $MgSO_4$
maximum pressure	40 bar
MWCO	150−300 Da sucrose & glucose
maximum temperature	90 °C
chlorine tolerance	1000 ppm.h
recommended pH	1−11

of neutral solutes consists of a Sepa CF II labscale 316 SS cell system (10), a feed tank (3) with a stainless steel immersed coil (5), and a volumetric pump (8) (cat pump 231, constant flow 9 L/mn). The closed loop of the feed solution is made of high temperature and pressure-resistant tubing (up to 60 °C and 20 bar). Only the part of the tubing between the pump and the Sepa CF system is stainless steel. The feed solution is heated or cooled in the 32 L feed tank by a circulating thermal bath (1) (Frigitherm-10 P-Selecta) by means of an immerged coil.

The temperature in the feed tank is measured and controlled by an external PT100 Prosensor probe (4) immerged in the feed solution. We also measure the retentate temperature when it is put back in the feed tank (2). The pressure of the feed solution and the retentate, modified by the valve (11), are given by pressure gauges (9). The permeate mass is measured by a balance (12) (Sartorius CP323S) at steady state, and the calculated mass flux is registered on a computer (13) via an RS232 output.

Membranes, Feed, and Solutes. The water used for pure water permeability measurements and for the preparation of feed solutions is purified water (5 MΩ) prepared using a commercial system (RIOS 8, Millipore Corp.). The tank was filled with 30 L of this water, and experiments were carried out using a constant concentration (1 g/L) of the four neutral solutes (listed in Table 1 along with their properties). We used the Desal5DK membrane in flat sheet form with 133 cm^2 measured effective membrane area. The membrane characteristics provided by the manufacturer are given in Table 2. For the measurements of the neutral solute concentrations, we used an Interferometer Refractometer (Optilab DSP, Wyatt Technology).

Membrane Pretreatment. Before using the new membranes for experiments, we treated them to eliminate chemical preservation products and compaction effects. The coupon was placed in the membrane cell (Osmonics Sepa CF II), and pure water was circulated for 2 h at 20 bar. This pressure was chosen greater than the maximum pressure used in permeation and rejection experiments (15 bar) and lower than the maximum pressure of 40 bar recommended by the manufacturer. Then, a circulation of a 1 g/L solution of the hydrophilic solute, glycerin, was performed for 4 h at low pressure (2 bar). Starting from this value, we progressively increased the pressure in steps of 2 bar every 5 min until reaching the maximum pressure of 15 bar. We then proceeded to a rinsing of the membrane with pure water for 1 h at 10 bar and ambient temperature. This protocol assures us of attaining the steady-state characteristics of the membrane.

This treatment was applied to each of the two coupons used in this work (cut from the same Desal5DK lot), and after each full solute experiment, we rechecked the pure water permeability. Figure 2 shows the permeability of a coupon measured by following this procedure. The permeability before treatment is found to be 8.33 L/(h.m^2 bar) and after treatment increases by 19%. We also show in this figure the pure water permeability after using glycerin as a solute and after experiments with glucose. After each solute measurement, pure water is circulated to rinse the membrane. There is less than 2.3% variation of pure water permeability, which is less than the estimated experimental error of 9%.

Experimental Procedures. For all the experiments carried out, the temperature effect was studied by increasing the temperature from the lowest (3 or 22 °C) to the highest (50 °C) value. The increase of temperature is made in a static way without circulating the feed solution. When the desired temperature is reached, the feed is set in circulation and the pressure is increased step by step from 5 to 15 bar. The circulation of the feed solution is maintained around 5 min until steady state is reached. Then, permeate mass is measured, and a 5 mL sample is collected. Finally, the collected solution is manually reintroduced after each experiment. The range of each operating parameter and the experimental errors are summarized in Table 3.

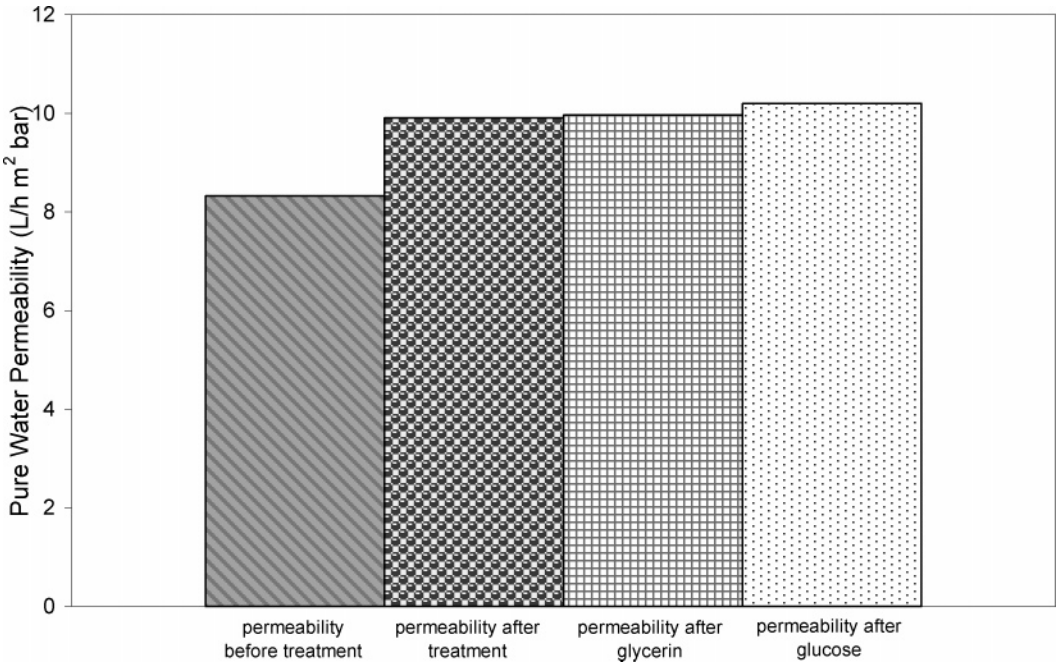

Figure 2. Variation of the pure water permeability, L_p^0 of the Desal5DK membrane at 30 °C before and after treatment and experimental work.

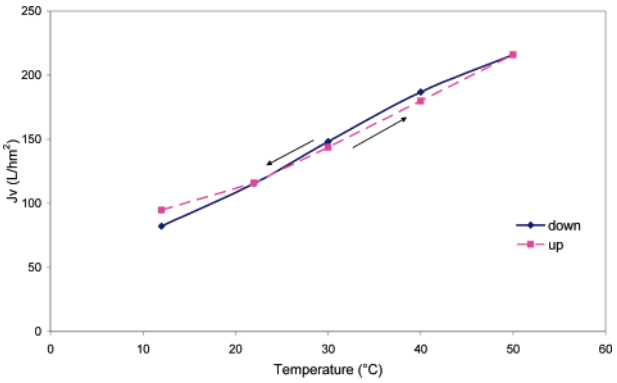

Figure 3. The pure water flux, j_v^w, as a function of temperature for a mean transmembrane pressure of 13 bar.

The feed solution circulates at a high constant tangential velocity (1.23 m/s), which allows us to neglect concentration polarization effects (consistent with the monotonically increasing rejection vs flux curves observed experimentally). The greatest feed recovery calculated is 0.7%, a value which validates our assumption of constant feed tank concentration even before manually reintroducing the permeate sample in the tank.

After the membrane treatment phase and the pure water tests, we studied the rejection of the solutes mentioned above (Table 1). For this purpose, we filled the tank with 30 L of pure water and then added the solute studied.

Experimental Results. *Hysterisis.* Pure water experiments were carried out with the Desal5DK membrane by increasing the temperature from 4 to 50 °C and then decreasing it back. The results presented in Figure 3, which show the water flux as function of the temperature at 13 bar, confirm that there is no noticeable hysterisis.

Effect of Temperature on Water Flux. In Figure 4, we show experiments realized at different temperatures and different applied pressures. For a given temperature, we see the expected linear increase of the permeate flux when the applied pressure varies from 5 to 15 bar. This indicates that membrane compaction is negligible in this pressure range. As the temperature increases from 3 to 50 °C, the slope of the linear evolution of the flux as a function of the applied pressure increases, and this increase corresponds to the increase of the membrane permeability.

Table 3. Estimated Errors for Operating Parameters

parameter	range	error
pressure	5−15 bar	6%
temperature	3−50 °C	±1
permeate flux	18−216 L/mn	±3%
feed concentration	1 g/L	±1.5%

This increase of the water permeability with temperature has been previously attributed in part to the temperature dependence of an intrapore viscosity that follows that of bulk water. In Figure 5, we show the normalized "bulk water viscosity" corrected permeability

$$\frac{L_p^0(T)\,\mu(T)}{L_p^0(T_0)\,\mu(T_0)} \tag{1}$$

obtained using our results for the Desal5DK and, for comparison, some previous results obtained using other nanofiltration membranes: homemade inorganic membranes denoted M1, M2, M3 (MWCO, respectively, of 200, 600, 2000),[9] and the Desal5DL.[10] We can see that, regardless of the type of membrane (inorganic or polymeric), the "bulk viscosity corrected" permeability cannot completely explain the increase of permeability with temperature. The largest residual temperature dependence appears to occur for the M1 membrane, which is said to possess the smallest pore diameter of all the membranes presented in Figure 5.

Effect of Temperature on Solute Rejection. Figure 6 shows the rejection of neutral solutes as a function of the permeate flux density obtained with the Desal5DK membrane. At a given temperature, as expected, neutral solute rejection first increases with flux density and then tends toward a high flux plateau. We also note a decrease of rejection with an increase in temperature for all the solutes studied. The strongest variations with temperature occur for the intermediate MW solutes, glucose and arabinose (the latter not shown in Figure 6 for clarity). For sucrose, the temperature has only a slight effect on rejection below 50 °C. The rejection curves for all solutes tend to limiting high flux values that decrease with temperature. If the effective solute size is assumed to be independent of temperature,

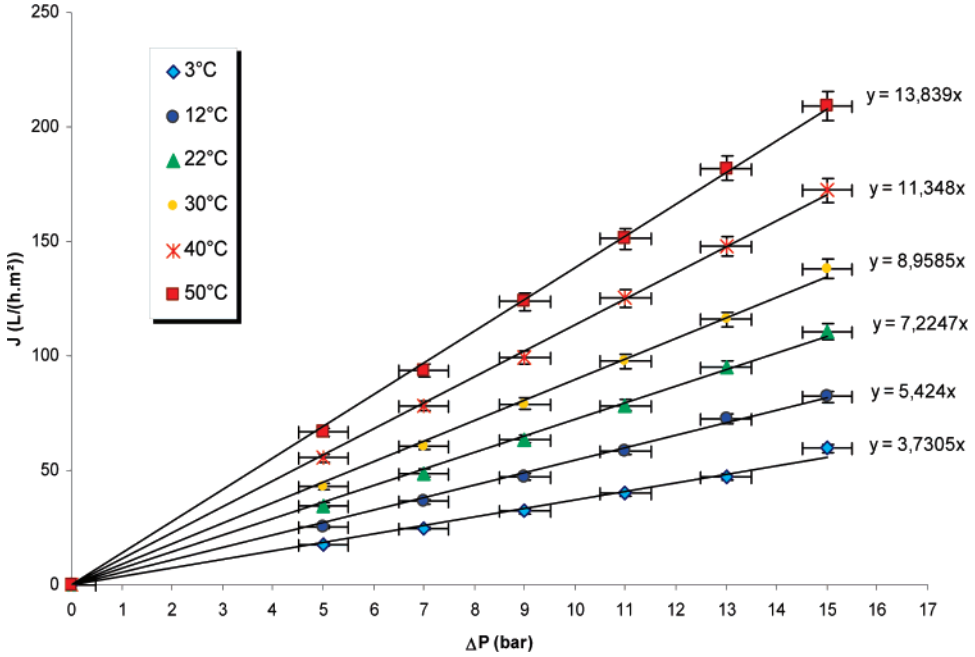

Figure 4. The pure water flux, j_v^w, as a function of the mean transmembrane pressure varying from 5 to 15 bar and for different temperatures (3 to 50 °C). The errors calculated for the pure water flux and the applied pressure are, respectively, 3% and 6.5%.

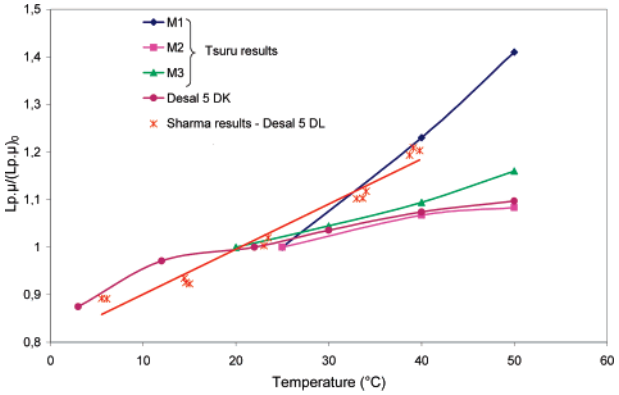

Figure 5. Corrected water permeability, μL_p^0, normalized with those at 23 °C,[9] 20 °C for M3, 25 °C for M1 and M2,[8] and 22 °C for our results with the Desal5DK membrane.

this implies that the MWCO of the membrane, and therefore the effective pore radius, increases with increasing temperature.

Role of Structural Parameters. The above experimental results for water permeability and neutral solute rejection (Figures 5 and 6) reveal that membrane structural parameters, such as the effective pore radius and thickness, may play an important role in determining the variation of membrane performance with temperature. Within the framework of the hindered transport theory, we now turn to a detailed examination of the role of these structural parameters in determining temperature-dependent membrane properties.

Theoretical Section

Hindered Transport Theory. *Neutral Solute Rejection.* In order to understand the effect of temperature on neutral solute rejection in nanofiltration, we employ the hindered transport (HT) theory developed for hard spheres in cylindrical pores and extend it to more complicated porous structures by introducing a tortuosity correction factor.[18] HT theory accounts for the steric and hydrodynamic interactions between solutes and pores. Although this continuum hydrodynamic approach will certainly break down for very small solutes (smaller than the solvent molecules, for example) in very small nanopores,[21] we assume, as is usual for NF modeling,[22] that it is a reasonable starting point for the nanofilters and solutes studied here (pore radius $r_p \approx 0.6$ nm and solute radii $r_s = 0.26 - 0.47$ nm).

Although the membranes studied have radii that are four times bigger than the radius of a solvent (water) molecule (~0.16 nm), and the solutes have radii that are two to three times bigger, the validity of the continuum hydrodynamic approach for such small particles is still an open question (although there is evidence that solutes in the bulk behave as hydrodynamic particles with no surface slip if they are 2 or 3 times bigger than the solvent molecules).[18] Despite these uncertainties, we believe that because of its conceptual simplicity the present approach is still a useful starting point in investigations of neutral solute rejection and could provide a suitable framework for unveiling any eventual internal incoherencies. Even in very small nanopores, outside the usual NF range, theoretical studies have been carried out to examine the role of purely entropic, excluded volume effects without the complications of other interactions.[21] Despite some interesting qualitative attempts to ascertain the role and importance of other, nonhindered transport, interactions between small solutes and nanopores, this is a difficult and still open problem. In ref 19, for example, a statistical analysis of experimental rejection data seemed to show that neutral molecules with high dipole moments have lower rejections than nonpolar neutral molecules of roughly the same size. One difficulty in establishing such a correlation is that it is very difficult to isolate the importance of any one component of the total solute−membrane interaction; in the case under consideration, one would need to compare the rejection of two neutral molecules that differ only in their dipole moment values. Since this is impossible to realize in practice (in reality, the molecules used in the comparison differed somewhat in size and shape), one must also be sure that other solute−membrane interactions are either nearly identical, such as the HT ones, or negligible. This difficulty has already been pointed

(21) Goulding, D.; Melchionna, S.; Hansen, J.-P. *Phys. Chem. Chem. Phys.* **2001**, *3*, 1644−1654.

(22) Palmeri, J.; Blanc, P.; Larbot, A.; David, P. *J. Membr. Sci.* **1999**, *160*, 141−170.

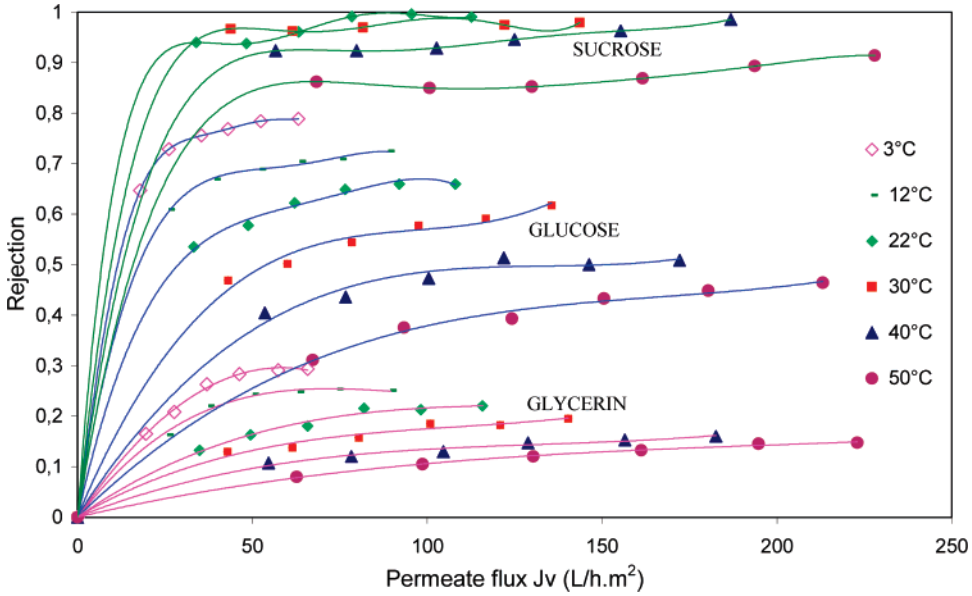

Figure 6. Rejection of glycerin, glucose, and sucrose as a function of the permeate flux density for the Desal5DK membrane for different temperatures.

out in ref 20, where it is stated that more complex solute−membrane interactions may complicate the interpretation of differences in neutral solute rejection data in terms of dipole interactions. The difficulty in going beyond qualitative studies of solute−membrane interactions, such as the one evoked above, is underlined by later work by the same authors: after acknowledging that for neutral solutes with not too high dipole moments the dipole interactions play only a secondary role, they resort to hindered transport models to analyze their neutral solute rejection data[20] with the solute radius and effective membrane pore radius being the only relevant parameters determining the limiting (high pressure) rejection.

In summary, we suppose that in the case of NF it is a reasonable starting point to adopt the hindered transport model to analyze neutral solute rejection and define a unique effective pore size, r_p, for realistic porous membranes (even ones whose structures differ considerably from a collection of straight cylindrical pores, which can be justified using percolation theory arguments).[20] This supposition has been tested extensively at ambient temperatures with a reasonably good positive result (see, for example, refs 20, 22, and references therein). Our goal here is to present a further test of this supposition by examining whether or not the hindered transport model retains its ability to provide a reasonable description of neutral solute rejection over a wide temperature range.

The radius of a neutral solute is estimated in terms of an equivalent hard sphere radius using the Stokes−Einstein equation

$$r_s = \frac{k_B T}{6\pi\mu(T)\, D_s(T)} \tag{2}$$

where T is the temperature, k_B is the Boltzmann constant, and D_s is the bulk diffusion coefficient. Once determined, we assume that the solute radius is independent of T, which implies that D_s varies as function of temperature according to $T/\mu(T)$.

We assume macroscopic one-dimensional transmembrane transport across a mesoscopically homogeneous membrane, which implies that transport coefficients are independent of position. The 3D volume-averaged convection−diffusion equation for the solute molar flux density, j_s, is given by

$$j_s = -\bar{D}_s \frac{d\bar{c}_s}{dx} + K_c \bar{c}_s j_v \tag{3}$$

where j_v is the volume flux density and $\bar{c}_s$ is the local averaged solute concentration within the membrane (moles per liter of pore volume), $\bar{D}_s$ is the effective solute diffusion coefficient, and K_c is the convective hindered transport factor (x, the transverse distance, varies from 0 to l_m, the physical membrane thickness). The intramembrane diffusivity, $\bar{D}_s = D^*_s\, \phi_p K_d/\tau_s$, depends on $D^*_s = D_s\mu/\mu_p$, an apparent bulk diffusivity (evaluated using the Stokes−Einstein equation with the pore solution viscosity μ_p instead of the bulk one), and K_d, the diffusive hindered transport factor. In an attempt to account for tortuosity effects that may be solute size dependent, we have introduced into $\bar{D}_s$ a tortuosity factor τ_s, which would be equal to 1 for a collection of straight cylindrical pores if the continuum hydrodynamic hypothesis were valid. The solute concentration in the membrane near the solution/membrane interfaces, $\bar{c}_s(0^+) = \Phi_s c_s^f$ and $\bar{c}_s(l_m^-) = \Phi_s c_s^p$, can be related to the external concentrations in the feed and permeate, c_s^f and c_s^p, using the solute partition coefficient, Φ_s. If we define a virtual equivalent "bulk" solute concentration in the membrane, $c_s(x)$, via $\bar{c}_s(x) = \Phi_s c_s(x)$, the solute flux density equation can be put into canonical Spiegler−Kedem[23] form

$$j_s = -P_s \frac{dc_s}{dx} + (1 - \sigma_s)\, c_s j_v \tag{4}$$

where

$$P_s = \Phi_s \bar{D}_s = \Phi_s D_s K_d l_m / l^s_{eff} \tag{5}$$

is the effective solute permeability with $l^s_{eff} = (l_m \tau_s \mu_p)/(\mu\phi_p)$ the effective membrane thickness for each solute and

$$\sigma_s = 1 - \Phi_s K_c \tag{6}$$

is the solute filtration reflection coefficient. The solute partition coefficient, Φ_s, takes into account all the interactions operating between the solute and the membrane (assuming, as we have done, that solute−solute interactions are negligible at the low

(23) Speigler, K. S.; Kedem, O. *Desalination* **1966**, *1*, 311.

concentrations studied here). We can put Φ_s in the following form by separating the steric part, Φ_{steric}, from the residual part of the total solute partition coefficient

$$\Phi_s = \Phi_{steric} \exp[-F_{res}/(k_B T)] \quad (7)$$

The steric part will depend on temperature if the effective pore radius does; the residual part depends on the ratio of total residual solute−membrane interaction free energy, F_{res}, and the temperature. The residual free energy F_{res} accounts for all nonsteric interactions, including the dipole one discussed in refs 19 and 20. The net effect on the solute partition coefficient of the residual free energy, upon an increase in temperature, depends on both the sign of F_{res} (repulsive if positive and attractive if negative) and how F_{res} varies with temperature. In this light, it would be interesting to analyze the different secondary interactions and their temperature dependencies to see what role they could play in explaining the commonly observed decrease of solute rejection with increasing temperature. Although such a study is outside the scope of the present work, we do note, however, that a freely rotating dipole (μ_D)−point charge (Q) interaction is attractive with a free energy proportional to $-\mu_D^2 Q^2/(\epsilon^2 k_B T d^4)$, where ϵ is the solvent dielectric constant and d is the separation. Although the situation is more complicated for membranes (the charge is spread out on the pore walls), we can assume that an analogous expression holds for freely rotating dipole (μ_D)−membrane interactions with Q replaced by a suitably defined effective membrane charge density, Q_{eff}. The quantity appearing in the Boltzmann factor, $-F_{dipole}/(k_B T)$, is therefore positive and proportional to $\mu_D^2 Q_{eff}^2$. The second (Boltzmann) factor in eq 7 thus increases with increasing μ_D, the solute partitioning increases, and therefore the rejection decreases, in agreement with experiment.[20] On one hand, if we assume that μ_D, ϵ, and Q_{eff} are temperature-independent, then $-F_{dipole}/(k_B T) \propto (k_B T)^{-2}$; the solute partitioning would then decrease with increasing temperature, and therefore the rejection would increase, contrary to what is observed experimentally. On the other hand, if μ_D, ϵ, and Q_{eff} are themselves temperature-dependent, the analysis becomes complicated. Although it would be interesting to carry out such an analysis for solutes with large dipole−membrane interactions, we do not believe these or other secondary (polarizability, hydration, etc.) effects to play an important role in the present study. The first major supposition made here is thus that the steric part to solute partitioning is dominant, and therefore the residual part plays only a negligible role, in agreement with the conclusions reached in ref 20.

If we assume that the transport coefficients, σ_s and P_s, are independent of solute concentration, we can then integrate the solute flux density equation (using the usual steady-state filtration boundary condition, $j_s = j_v c_s^p$) to find the solute rejection

$$R = 1 - \frac{c_s^p}{c_s^f} = \frac{(1-G)\sigma_s}{1-\sigma_s G} \quad (8)$$

where $G = \exp(-\mathrm{Pe}_s)$ with

$$\mathrm{Pe}_s = j_v l_m \left(\frac{1-\sigma_s}{P_s}\right) = \frac{j_v l_{eff}^s K_c}{D_s K_d} \quad (9)$$

the Péclet number.

The rejection is an increasing function of Pe_s. At low flux (low Péclet number), the rejection increases linearly with j_v or Pe_s

$$R \approx \frac{\sigma_s \mathrm{Pe}_s}{1-\sigma_s} = \frac{\sigma_s l_m j_v}{P_s} \quad (10)$$

At high flux (high Péclet number), the rejection tends toward its limiting value, independent of Pe_s and equal to the filtration reflection coefficient

$$R^\infty = \sigma_s \quad (11)$$

For $\mathrm{Pe}_s > 1$, the rejection is close to the limiting one, and for $\mathrm{Pe}_s \ll 1$, the rejection is a linearly increasing function of Pe_s.

The second major supposition made is that, although real NF membranes have complicated structures, the key parameters entering the HT theory (K_d, K_c, and Φ_{steric}) can be estimated using the much simpler and well-known cylindrical pore HT theory. The reason for this supposition is simply that little or nothing is known about hindered solute transport in more complicated pore geometries (cf. ref 24). The hope, borne out partly by previous applications of the theory, is that with an appropriate choice of effective pore size and effective membrane thickness the cylindrical pore HT theory can give a reasonable description of neutral solute rejection by nanofilters.

For cylindrical pores, the HT theory predicts that (i) the steric partition coefficient is given by $\Phi_s^{cyl} = (1-\lambda_s)^2$, where $\lambda_s = r_s/r_p$ is the ratio of solute to pore radius and (ii) the hindered transport factors, K_d^{cyl} and K_c^{cyl} depend only on λ_s (see Appendix 1). This in turn implies that for cylindrical pores σ_s and P_s depend on, among other things, solute and pore size via $K_d^{cyl}(\lambda_s)$ and $K_c^{cyl}(\lambda_s)$, respectively. In principle, we should also introduce correction factors in order to account for the expected differences between hindered solute diffusion, convection, or steric partitioning in real porous nanofilters and simplified membrane models possessing straight cylindrical pores. Due to the nearly complete lack of knowledge concerning these correction factors, we will not attempt to do this here. It should be kept in mind, however, that the pore size and the membrane thickness obtained by fitting the cylindrical pore HT theory to neutral solute NF rejection data are truly effective parameters, for their fitted values will indirectly reflect the contributions of the unaccounted for correction factors. Indeed, the absence of these correction factors in the transport model used here could help explain in a reasonable way the unexpected behavior we find below for variations of membrane thickness as a function of temperature and/or solute size.

Within the scope of the cylindrical pore HT theory, the effective solute permeability, filtration reflection coefficient, and Péclet number are obtained by using K_d^{cyl}, K_c^{cyl}, and Φ_s^{cyl} in eqs 5, 6, and 9:

$$P_s = D_s \Phi_s^{cyl} K_d^{cyl} l_m / l_{eff}^s \quad (12)$$

$$\sigma_s^{cyl} \equiv 1 - \Phi_s^{cyl} K_c^{cyl} \quad (13)$$

and

$$\mathrm{Pe}_s = \frac{j_v l_{eff}^s K_c^{cyl}}{D_s K_d^{cyl}} \quad (14)$$

According to eq 13, σ_s (and therefore R^∞) will be temperature-dependent only if r_p is. On the other hand, at fixed j_v a temperature dependence of r_p, l_{eff}^s, and D_s could potentially influence the

(24) Kluijtmans, S. G. J. M.; Philipse, A. P. *Langmuir* **1999**, *15*, 1896.

Péclet number and therefore the solute rejection, provided that Pe_s is sufficiently low that the high flux plateau has not yet been attained.

In summary, at any given temperature we assume that it is possible to characterize a nanofilter by a single effective pore size, r_p (independent of solute), and an effective membrane thickness for each solute, $l^s_{eff} \geq l_m$, with all parameters being determined simultaneously by fitting the experimental neutral solute rejection vs j_v data to the HT model given by eqs 8, 13, and 14. In general, we may expect that r_p and l^s_{eff} will be temperature-dependent, because of temperature-dependent membrane structural modifications, for example, or, in the case of l^s_{eff}, because μ_p may differ in temperature dependence from μ. More generally, r_p and l^s_{eff} could also take on an apparent temperature dependence in order to try to *compensate* for any effect not accounted for in the basic model, including a possible breakdown of the continuum hydrodynamic hypothesis in nanopores or the neglect of residual (nonsteric) interactions.

Water and Solution Flux. The pure water flux is

$$j_v^w = L_p^0 |\Delta P| \tag{15}$$

where ΔP is the transmembrane pressure difference and L_p^0 is the pure water permeability, given by

$$L_p^0 = \frac{r_p^2}{8\mu l^w_{p,eff}} \tag{16}$$

where $l^w_{p,eff} = (l_m \tau_w \mu_p)/(\mu \phi_p)$ is the effective membrane thickness associated with pure water permeability with τ_w a generalized "permeability" tortuosity (not necessarily equal to any of the τ_s). For continuum hydrodynamic flow in a collection of straight cylindrical pores $l^w_{p,eff}$ reduces to l_m/ϕ_p. In general, $l^w_{p,eff}$ accounts for all possible deviations of behavior from continuum hydrodynamics in straight cylindrical pores, including tortuosity effects and differences between bulk and pore viscosity.

After the pore radius has been determined from neutral solute rejection data (see above), the volume flux density vs pressure data can be used with eqs 15 and 16 to evaluate the effective thickness of the membrane for the permeability, $l^w_{p,eff}(T)$, as a function of temperature.

In the experiments carried out here, solute concentrations are sufficiently low (1 g/L) for both solute−solute interactions and osmotic pressure effects to be negligible (solute molar concentrations are less than 10^{-2} mol/L and solute volume fractions are less than 8×10^{-4}). We therefore assume that volume flux density for solutions, given by[18]

$$j_v = -L_p^s(\Delta P - \sum \sigma_d^s \Delta \Pi^s) \tag{17}$$

within the framework of the hindered transport model can be approximated by the pure water flux, j_v^w, i.e., $j_v \approx j_v^w$ (L_p^s is the solution permeability, σ_d^s is the solute osmotic reflection coefficient, and $\Delta\Pi^s$ is the osmotic pressure difference across the membrane due to solute s). To verify that this assumption is reasonably well satisfied for a given solute solution, we write

$$j_v \approx L_p^s |\Delta P| \tag{18}$$

for the volume flux density of the solution, where

$$L_p^s = \frac{r_p^2}{8\mu l^s_{p,eff}} \tag{19}$$

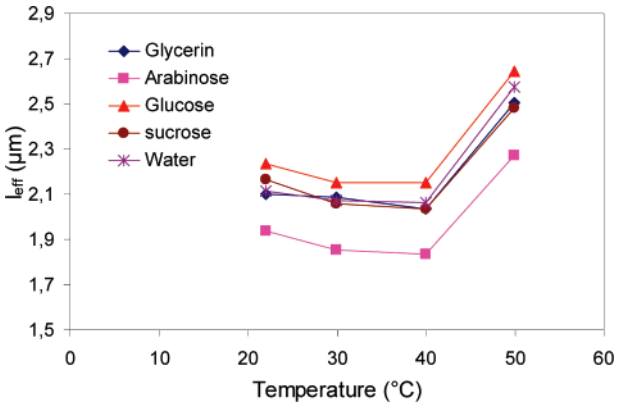

Figure 7. Effective thickness estimated from pure water, $l^w_{p,eff}$, and solution permeability, $l^s_{p,eff}$ (four solute solutions) as a function of temperature.

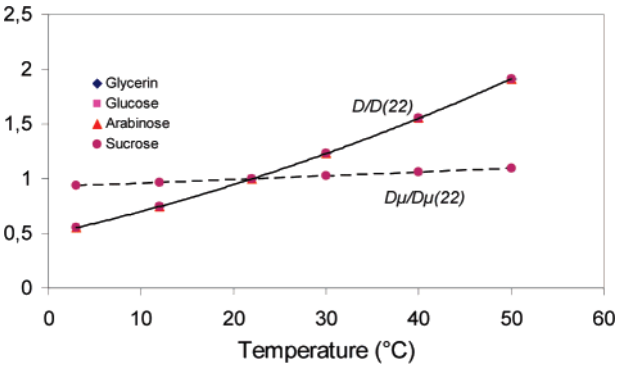

Figure 8. Normalized bulk diffusion coefficient $D_s(T)/D_s(22)$, and normalized product of viscosity and diffusion coefficient, $\mu(T)D_s(T)/[\mu(22)D_s(22)]$, as a function of the temperature.

with $l^s_{p,eff}$ the effective membrane thickness associated with solution permeability. In Figure 7, we compare $l^w_{p,eff}$ with $l^s_{p,eff}$ for the four solutes. In confirmation of our assumption, we observe relatively good agreement between all the effective membrane thicknesses associated with the permeability (with the biggest discrepancy appearing for arabinose; see Figure 7).

Modeling Protocol. *Solute Rejection as a Function of* j_v. Our strategy for modeling the solute rejection as a function of j_v will involve three different levels of analysis concerning the temperature dependence of D_s, r_p, and l^s_{eff}:

Level 1. D_s temperature-dependent (from eq 2); r_p and l^s_{eff} independent of temperature and adjusted at 22 °C.

Level 2. D_s and r_p temperature dependent with r_p adjusted at each temperature studied; l^s_{eff} independent of temperature and adjusted at 22 °C.

Level 3. D_s, r_p, and l^s_{eff} temperature-dependent (the latter two being adjusted at each temperature studied).

The reason for this analysis in three steps is to clearly show that only when the effective pore radius and membrane thickness are allowed to vary with temperature can a good model fit be obtained.

By reasoning at level 1, we can see that at fixed volume flux density, j_v, the solute rejection, R, should decrease with increasing temperature. The reasoning goes as follows: at this level, l^s_{eff} and σ_s are considered constant, thus the only temperature dependence enters via the bulk diffusivity, D_s, which is an increasing function of T (Figure 8). Because Pe_s obeys $Pe_s \propto 1/D_s$ (eq 14), it is a decreasing function of T, and because R decreases with decreasing

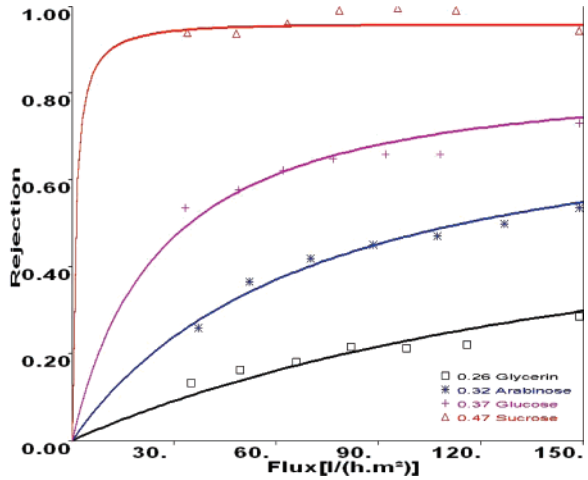

Figure 9. Rejection vs j_v: model fit at $T = 22$ °C.

Pe_s, R is also a decreasing function of T. We conclude that the bulk temperature dependence of the solute diffusivity could explain part of the commonly observed experimental trend that solute rejection decreases with increasing T.

Solute Rejection and Solution Volume Flux Density as a Function of Pressure. Our strategy for modeling the solute rejection as a function of pressure ΔP also involves three different levels of analysis, but now concerning the temperature dependence of μ, D_s, r_p, l^s_{eff}, and $l^w_{p,eff}$:

1. μ and D_s temperature-dependent; r_p, l^s_{eff}, and $l^w_{p,eff}$ independent of temperature and adjusted at 22 °C.

2. μ, D_s, and r_p temperature-dependent and with r_p adjusted at each temperature; l^s_{eff} and $l^w_{p,eff}$ independent of temperature and adjusted at 22 °C.

3. μ, D_s, r_p, l^s_{eff}, and $l^w_{p,eff}$ temperature-dependent with r_p, l^s_{eff}, and $l^w_{p,eff}$ adjusted at each temperature.

For fixed pressure, $|\Delta P|$, we can also argue that at level 1 R should decrease with increasing temperature. By combining eqs 14−16, we obtain

$$Pe_s \approx \frac{1}{8}\left(\frac{l^s_{eff}}{l^w_{p,eff}}\right)\left(\frac{K_c^{cyl}}{K_d^{cyl}}\right)\left(\frac{r_p^2 \Delta P}{D_s \mu}\right) \qquad (20)$$

where we have assumed, as stated earlier, that $l^s_{p,eff} \approx l^w_{p,eff}$. All the possibly temperature dependent parameters (μ, D_s, r_p, l^s_{eff}, and $l^w_{p,eff}$) could potentially influence the Péclet number and therefore the rejection, provided that Pe_s is sufficiently low that the high flux plateau has not yet been attained. Because the product $D_s\mu$ increases with T and r_p, l^s_{eff}, and l^{per}_{eff} are assumed constant at level 1, Pe_s and therefore R again decrease with increasing T. Because $D_s\mu$ (see eq 2) is proportional to the absolute temperature and this temperature only increases slightly over the temperature range studied (much less than D_s alone; see Figure 8), we expect the level 1 rejection predictions at constant pressure to be practically independent of temperature for T between 22 and 50 °C. Because this level 1 prediction is not in accordance with experimental trends (see below), the temperature dependence of r_p, l^s_{eff} will play an important role in our analysis.

Theoretical Analysis of Experimental Results. We would now like to address the question of whether the known bulk temperature dependences of μ and D_s are sufficient to account quantitatively for the temperature dependence of the solute rejection, R, and solution permeability; and, if not, what are the roles played by r_p and l^s_{eff}?

Table 4. Coefficient of Determination, R^2, for the Model Fit; Fitted Membrane Pore Radius and Standard Error; and Fitted Membrane Effective Thickness, l_{eff}, and Standard Error, σ, for Four Solutes at Four Temperatures (level 3)[a]

T (°C)	R^2	r_p (nm)	σ (nm)
22	0.993	0.58	0.03
30	0.994	0.58	0.02
40	0.991	0.59	0.03
50	0.996	0.67	0.02

l_{eff} (μm) [σ (μm)]			
glycerin	arabinose	glucose	sucrose
1.31 [0.33]	0.98 [0.30]	0.89 [0.34]	0.69 [0.82]
1.13 [0.21]	0.67 [0.14]	0.65 [0.19]	0.65* [*]
0.92 [0.30]	0.46 [0.18]	0.51 [0.27]	0.57 [1.07]
1.46 [0.23]	0.56 [0.09]	0.97 [0.20]	1.80 [1.20]

[a] The symbol * means that a fitted value could not be obtained with a reasonable standard error, and therefore a value compatible with the experimental data was chosen by hand.

Solute Rejection as a Function of j_v. We first present our analysis of the rejection data obtained using the Desal5DK membrane at four different temperatures: $T = 22$, 30, 40, and 50 °C. In Figure 9, we show the experimental rejection data for the four neutral solutes (glycerin, arabinose, glucose, and sucrose) obtained at 22 °C, as well as the curves obtained by fitting the HT model (see Appendix 2 for a discussion concerning the fitting procedure and a comparison between the method used here and the one used in ref 20). We find that the fit of the model to the data is very good: the fitted pore size is $r_p = 0.58 \pm 0.03$ nm, and the l^s_{eff} values are in the 0.7−1.3 μm range and decrease with increasing solute size or molecular weight (see Table 4). (It should be noted that the symbols farthest to the right and just below the NanoFlux simulation curves are not experimental data points, but serve rather to identify the curves, using the legend provided.) These values are consistent with the actual NF layer thickness, $l_m \approx 0.4$ μm, estimated using electron microscopy. This type of behavior for l^s_{eff} has often been observed in NF experiments carried out near room temperature. We note that the sucrose rejection is close to its high flux limiting value at all the pressures studied, and therefore the standard error associated with the fitted value of l_{eff} is larger than the fitted value itself. The rejections of the other three solutes, on the other hand, are in the intermediate range between the linear increase expected at low j_v and the limiting plateau expected at high j_v (the linear and intermediate rejections are controlled by the ratio $\lambda_s = r_s/r_p$ and l^s_{eff} via σ_s and P_s, and the high flux limiting plateau is controlled uniquely by λ_s via σ_s). Although the standard errors for these last three solutes (between 25% and 38%) are lower than for sucrose, the differences in l_{eff} between these solutes themselves are at or beyond the limit of statistical significance. Thus, any conclusion based on a physical interpretation of the differences between the fitted values of l_{eff} should be treated with caution (more data points on the rising part of the rejection curve for all the solutes would be needed to obtain more precise values of l_{eff}).

Level 1. In Figure 10a−c, we present the level 1 HT model predictions for $T = 30$, 40, and 50 °C, respectively. By keeping r_p and l^s_{eff} fixed at their fitted $T = 22$ °C values, we observe that, although the predicted solute rejections do decrease with increasing T (due to the increase in bulk diffusivity D_s; see above), this decrease is not strong enough to explain the experimental results. The widening gap between the model predictions and experiment as T increases leads us to conclude that, within the scope of the HT model used here, r_p and/or l^s_{eff} cannot be considered independent of T.

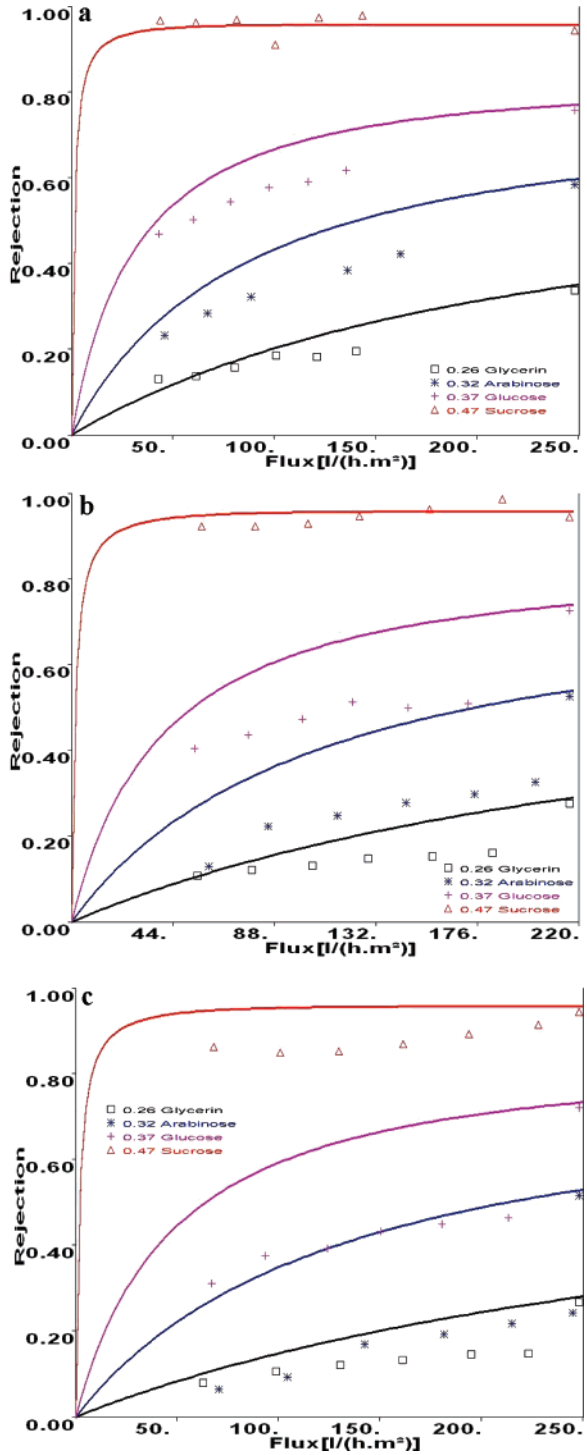

Figure 10. Rejection vs j_v: level 1 model predictions at T = (a) 30, (b) 40, and (c) 50 °C.

Level 2. The level 2 HT model predictions for T = 30, 40, and 50 °C were obtained by keeping the effective thicknesses, l_{eff}^s, fixed at their fitted T = 22 °C values and adjusting the pore radius at each temperature studied. Although the predicted solute rejections are now in generally better agreement with experiment, there are still noticeable discrepancies (for the sake of brevity, we omit the detailed level 2 "rejection vs volume flux density" plots; level 2 results will be compared below with levels 1 and 3 results at one value of volume flux density and one value of pressure). At level 2, the adjusted effective pore size, r_p, increases linearly with temperature, going from $r_p = 0.58 \pm 0.03$ nm at 22 °C to $r_p = 0.665 \pm 0.007$ nm at 50 °C (see Figure 11 and

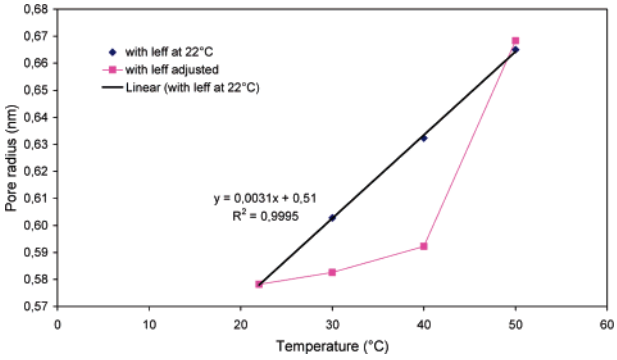

Figure 11. Evolution of pore radius, r_p, with temperature: level 2 (◆) and level 3 (■).

Table 5. Fitted Pore Radius and Standard Error as Function of Temperatures (level 2)

T (°C)	r_p (nm)	σ (nm)
22	0.580	0.03
30	0.603	0.004
40	0.632	0.006
50	0.665	0.007

Table 5). The standard errors are sufficiently small at T = 30, 40, and 50 °C for this increase to be statistically significant (we obtain smaller standard errors at 30, 40, and 50 °C because at level 2 there is only fitting parameter for these temperatures, with the l_{eff}^s values being held fixed at their T = 22 °C values). This behavior could be due to thermal dilation of the membrane structure. Although the agreement between the model results and experiment is fairly good at 30 °C for all four solutes, the agreement is poor at higher T for arabinose and to a lesser extent glucose. We can conclude that within the scope of the HT model used here l_{eff}^s cannot be considered independent of T.

Level 3. In Figure 12a−c, we present the level 3 HT model predictions for T = 30, 40, and 50 °C, respectively. By adjusting the effective pore radius, r_p, and membrane thicknesses, l_{eff}^s, at each temperature studied we obtain the results presented in Figures 11 and 13 and Table 4. At 30, 40, and 50 °C, there is now as good an agreement between the model and experiment as there was at 22 °C. At level 3, we can conclude that within statistical error the adjusted r_p is roughly constant between 22 °C and (at least) 40 °C, going from $r_p = 0.58 \pm 0.03$ nm at 22 °C to $r_p = 0.59 \pm 0.03$ nm at 40 °C. Somewhere above 40 °C, there is a steep, statistically significant, rise to $r_p = 0.67 \pm 0.02$ nm at 50 °C (more data would be needed at temperatures between 40 and 50 °C to uncover the details of this rapid rise). This behavior shows a nonlinear type of thermal dilation of the membrane structure that one would hope could be explained in terms of the physical properties of the polymer making up the membrane. For T = 22, 30, 40, and 50 °C, the fitted l_{eff}^s values are in the 0.5−2 μm range, consistent with the actual estimated NF layer thickness of $l_m \approx 0.4$ nm. For these temperatures, the standard errors for sucrose are again very large; although the standard errors for the other three solutes are much smaller than for sucrose, the differences between these solutes themselves are again almost all at or beyond the limit of being statistically significant. Although we will attempt to derive some general trends from the fitted values of l_{eff}^s, we must keep in mind that any conclusions derived from differences between the fitted values of l_{eff}^s are tentative ones.

With the above caveat in mind, we observe that, unlike what occurs at 22 °C (where l_{eff}^s decreases with increasing solute size),

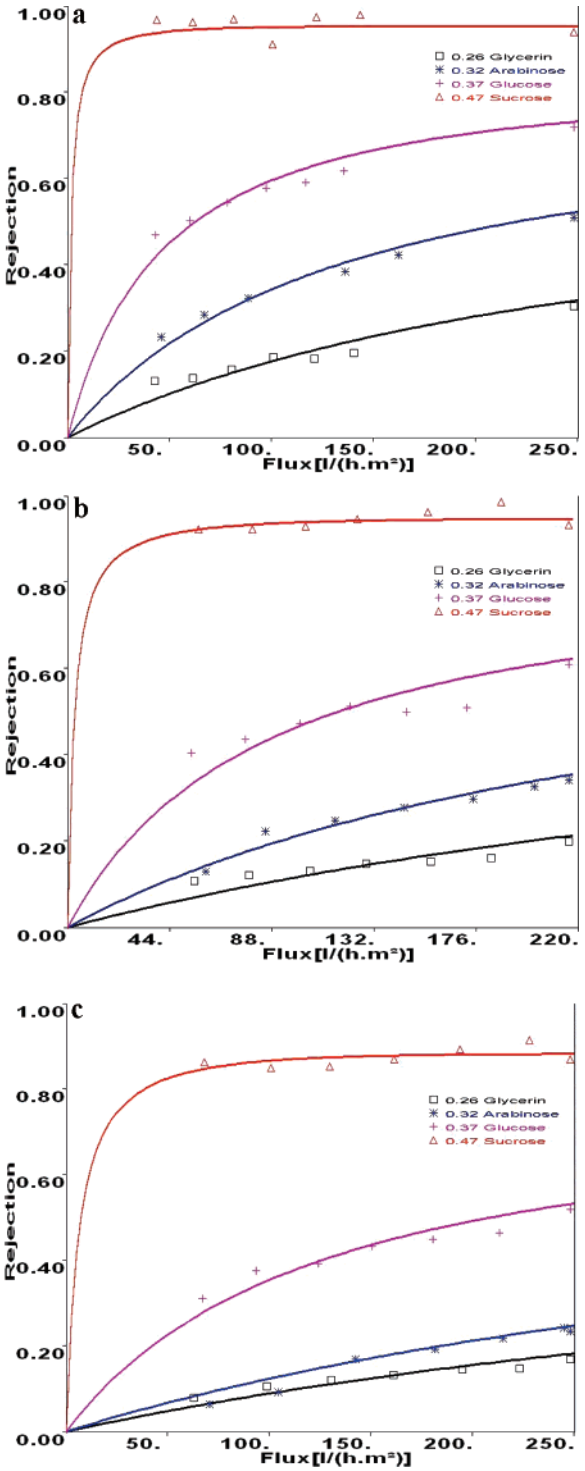

Figure 12. Rejection vs j_v: level 3 model predictions at T = (a) 30, (b) 40, and (c) 50 °C

at the higher temperatures studied there appears to be a non-monotonic behavior as a function of solute radius (with a minimum between glycerin and glucose; see Table 4 and Figure 13a). For all the solutes studied, there also appears to be a non-monotonic behavior for l^s_{eff} as a function of temperature. For the four temperatures studied, we observe a decrease from 22 to 40 °C and then an increase upon going from 40 to 50 °C (see Table 4 and Figure 13). If corroborated by more extensive measurements (coupled with more precise model fitting), these trends might furnish information on the difference between the diffusive hindrance factor for the real nanofilter studied, K_d, and the

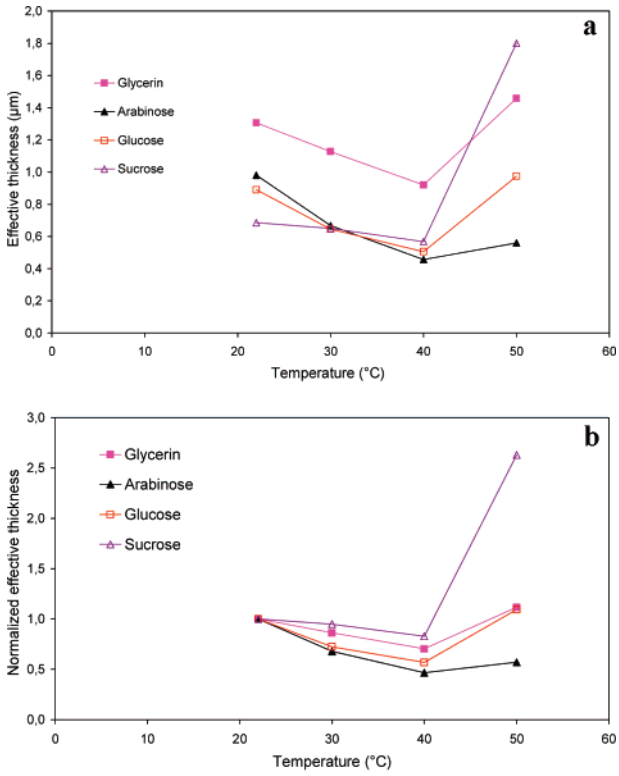

Figure 13. (a) Effective membrane thickness l^s_{eff} vs temperature (from rejection for four solutes). (b) Normalized thickness $l^s_{eff}(T)/l^s_{eff}(22\ °C)$ vs temperature.

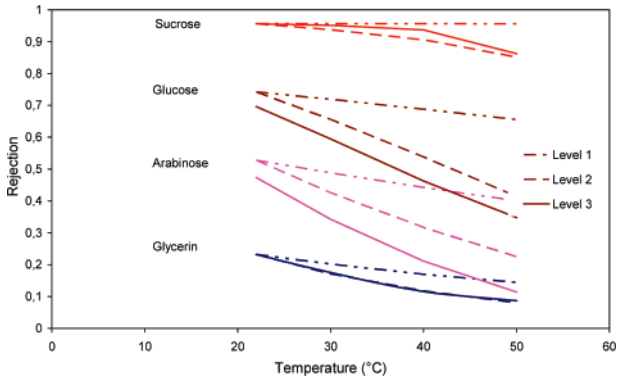

Figure 14. Rejection vs temperature at fixed volume flux density (j_v = 100 L/(h m^2)) (four solutes, three levels of analysis).

cylindrical pore form, K_d^{cyl}, actually used here in the HT theory. Unfortunately, very little theoretical and experimental work has been performed on hindered transport in real porous media (with noncylindrical pore geometries). There are some experimental results, however, that suggest that non-monotonic behavior for l^s_{eff} may be physically plausible: if we assume that $K_d/K_d^{cyl} = l_m/l^s_{eff}$ (i.e., $K_c \approx K_c^{cyl}$) in the Péclet number (eq 14), then an analysis of the experimental diffusion data presented in ref 24 for small solutes in micrometer-sized spherical grain packings does indeed show non-monotonic variations of l^s_{eff} with solute radius.[25]

Solute Rejection at Fixed Volume Flux Density. In Figure 14, we present the levels 1−3 model solute rejections as a function of temperature at fixed volume flux density (j_v = 100 L h^{-1} m^{-2}). We recall that the level 3 model results for rejection are in very good agreement with experiment (Figures 9 and 12) and can thus be considered reliable interpolated values at this volume

(25) Palmeri, J. et al. Unpublished results, 2006.

flux density (for which we do not necessarily have experimental rejection results, the rejection being measured at fixed pressure and not fixed volume flux density).

Because the sucrose rejections are on the high flux limiting plateau at this volume flux density, we do not expect a change in Pe_s with T to have any effect on rejection (only the reflection coefficient, σ_s, will play a significant role). The three smaller solute (glucose, arabinose, glycerin) rejections, however, are in the intermediate regime where changes in both Pe_s and σ_s with temperature could play a significant role (cf. eqs 9 and 10). Because D_s increases with T (Figure 8), the ensuing decrease in Pe_s

$$Pe_s \propto \frac{1}{D_s} \tag{21}$$

at level 1 therefore leads to a substantial decrease in rejection for glucose, arabinose, and, glycerin, but not sucrose. This decrease is not, however, sufficient to account for the experimental results (level 3 curves in Figure 14).

At level 2, besides the non-negligible influence of D_s, r_p also changes with temperature (Figure 11 and Table 5). The changes in r_p influence both $\sigma_s(\lambda_s)$ and

$$Pe_s \propto \left[\frac{K_c^{cyl}(\lambda_s)}{K_d^{cyl}(\lambda_s)}\right] \times \frac{1}{D_s} \tag{22}$$

via λ_s. The increase of r_p with T leads to a decrease in λ_s and therefore decreases in σ_s and Pe_s, both leading to lower rejection (the ratio K_c^{cyl}/K_d^{cyl} is a monotonically increasing function of λ_s). Although the increase in r_p with T reinforces the drop in rejection due to the increase in D_s already noted at level 1, it is clear from Figure 14 that these two effects alone are not capable of accounting for the experimental results. In order to do so, we must include the temperature dependence of the effective membrane thicknesses (level 3).

At level 3, Pe_s is also influenced by the temperature dependence of l_{eff}^s

$$Pe_s \propto l_{eff}^s \times \left[\frac{K_c^{cyl}(\lambda_s)}{K_d^{cyl}(\lambda_s)}\right] \times \frac{1}{D_s} \tag{23}$$

The changes in rejection as a function of T will now also depend on how l_{eff}^s changes with temperature. In Figure 13 and Table 4, we observe that l_{eff}^s decreases between 22 and 40 °C and then increases going from 40 to 50 °C. Thus, over the temperature range between 22 and 40 °C, all three factors in eq 23 work in tandem to decrease Pe_s (and thus rejection) with increasing T. This decrease in Pe_s will only have a strong influence on those solutes whose rejections are not on the limiting high flux plateau (the three smallest). The decrease in Pe_s is the predominant effect influencing the drop in rejection of the three smallest solutes between 22 and 40 °C, because r_p changes only slightly (and therefore σ_s varies little) in this temperature range. In going from 40 to 50 °C, the increase in l_{eff}^s for all four solutes counterbalances the decrease in Pe_s due to the second and third terms in eq 23 (Figure 15). This attenuates the decrease in rejection due to the decrease in Pe_s and indicates that the predominant effect on rejection in going from 40 to 50 °C is the decrease in σ_s due to the abrupt increase in r_p (see Figure 11).

Water and Solution Volume Flux Density. In an attempt to understand the temperature dependence of the water permeability,

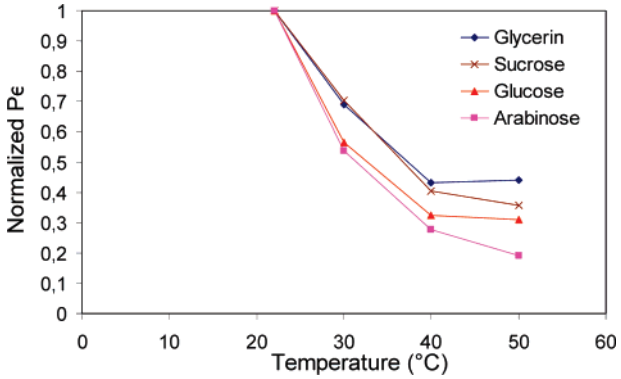

Figure 15. Evolution with temperature of the normalized Péclet number, $Pe_s(T)/Pe_s(22\ °C)$, for four solutes at fixed $j_v = 100$ L/(h m^2).

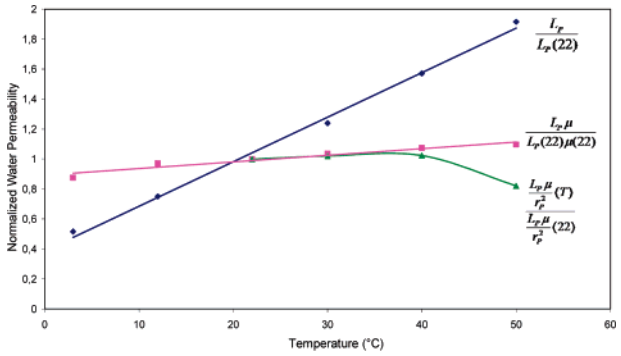

Figure 16. Water permeability normalized in different ways as a function of temperature for the Desal5DK membrane.

L_p^0, we present it in Figure 16 normalized in different ways. With our approach (eq 16), there are three parameters that could potentially contribute to the temperature dependence of L_p^0: μ, r_p, and $l_{p,eff}^w$. Although in the literature, normally only the first parameter, the bulk viscosity, is considered to depend on temperature, the temperature dependence of r_p and $l_{p,eff}^w$ could also influence j_v. Furthermore, eq 16 implies that the quantity

$$L_p^0(T)\,\mu(T)\,r_p^{-2}(T)\,l_{p,eff}^w(T) \tag{24}$$

but not necessarily $L_p^0(T)\,\mu(T)$ or $L_p^0(T)\,\mu(T)\,r_p^{-2}(T)$, should be independent of T.

The data for $L_p^0(T)/L_p^0(22\ °C)$ show a strong increase of nearly 400% in going from 3 to 50 °C (Figure 16). This strong increase is commonly observed for nanofilters and the question arises of whether or not it can be simply accounted for by the temperature dependence of the bulk viscosity. In Figure 16, we recall the residual temperature dependence of "bulk viscosity corrected" permeability (cf. Figure 5)

$$\frac{L_p^0(T)\,\mu(T)}{L_p^0(22\ °C)\,\mu(22\ °C)} \tag{25}$$

In this case, the residual temperature dependence is relatively weak but non-negligible (20% variation between 3 and 50 °C). We next plot the residual temperature dependence of

$$\frac{L_p^0(T)\,\mu(T)\,r_p^{-2}(T)}{L_p^0(22\ °C)\,\mu(22\ °C)\,r_p^{-2}(22\ °C)} \tag{26}$$

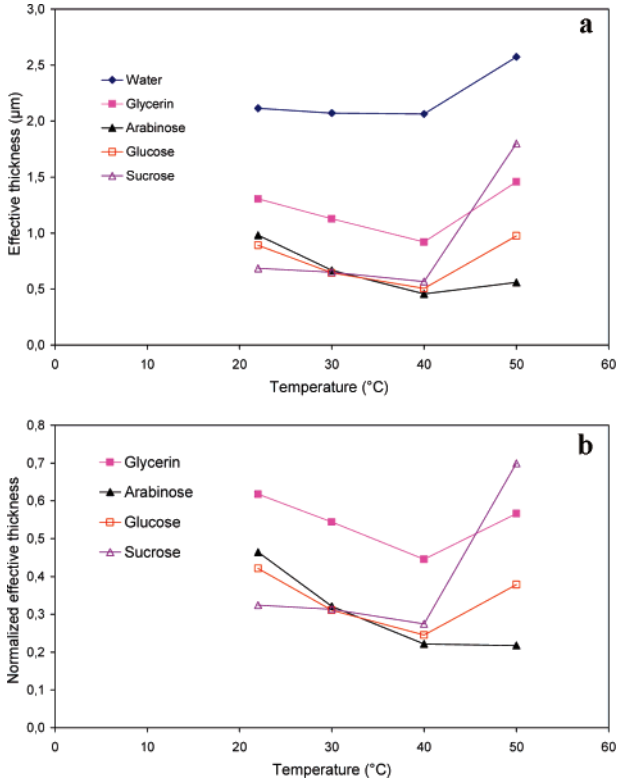

Figure 17. (a) Evolution with temperature of the effective thickness, l^{s}_{eff}, for four solutes (from rejection) and water, $l^{w}_{p,eff}$ (from permeability). (b) Evolution with temperature of the normalized effective thickness, $l^{s}_{eff}(T)/l^{w}_{p,eff}(T)$ for four solutes.

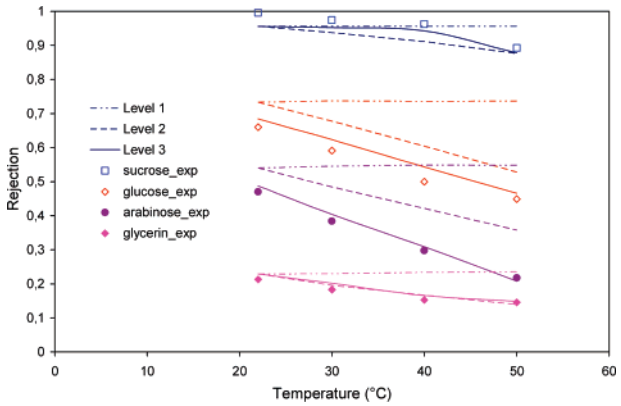

Figure 18. Rejection vs temperature at fixed pressure = 13 bar (four solutes, three levels of analysis).

but only for temperatures for which we possess r_p values (22 to 50 °C; see Table 4). Although the increase in r_p at level 3 between 22 and 40 °C tends to correct the residual temperature dependence found using eq 25, we observe an overcompensation at 50 °C. This suggests that the temperature dependence of $l^{w}_{p,eff}$ cannot be neglected. In the final step, we therefore introduce $l^{w}_{p,eff}$, which is defined so that

$$\frac{L^{0}_{p}(T)\,\mu(T)\,r_{p}^{-2}(T)\,l^{w}_{p,eff}(T)}{L^{0}_{p}(22\ °C)\,\mu(22\ °C)\,r_{p}^{-2}(22\ °C)\,l^{w}_{p,eff}(22\ °C)} = 1 \quad (27)$$

In Figure 17, we compare $l^{w}_{p,eff}$ and l^{s}_{eff} as a function of T and observe that $l^{w}_{p,eff}$ decreases slightly between 22 and 40 °C and then increases in going from 40 to 50 °C. This behavior for $l^{w}_{p,eff}$

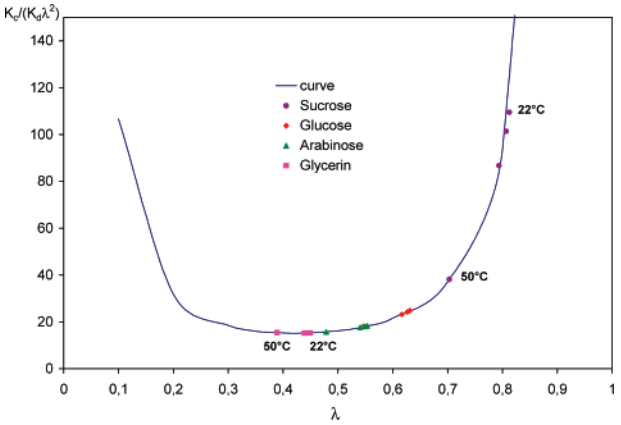

Figure 19. Normalized hindrance factors $K_c^{cyl}/(K_d^{cyl}\lambda_s^2)$ vs $\lambda_s = r_s/r_p$ (hindered transport theoretical curve and data for four solutes at four temperatures: 22, 30, 40, and 50 °C).

follows the tendencies already seen for l^{s}_{eff}. From the above results, we conclude that the temperature dependence of the bulk viscosity allows one to explain most, but not all, of the temperature dependence of the water permeability. Furthermore, the residual temperature dependence that remains after incorporating the bulk viscosity cannot be completely accounted for by the temperature dependence of the pore size, r_p, alone, for we have found it necessary to introduce a temperature-dependent effective membrane thickness, $l^{w}_{p,eff}$. This effective thickness is an adjustable parameter that attempts to account for all phenomena influencing the water permeability but not already accounted for via μ and r_p.

Solute Rejection as a Function of Pressure. In Figure 18, we present the experimental and levels 1−3 model solute rejections as a function of temperature at a fixed pressure of 13 bar.

Because the product $D_s\mu$ increases only very slowly with T over the temperature range studied (Figure 8), we see, as expected, that the level 1 predictions (σ_s invariant and $Pe_s \propto (D_s\mu)^{-1}$) are practically independent of temperature between 22 and 50 °C. At level 2, besides the negligible influence of $D_s\mu$, only r_p changes with temperature (Figure 11 and Table 5). The changes in r_p influence $\sigma_s(\lambda_s)$ and Pe_s

$$Pe_s \propto \left[\frac{K_c^{cyl}(\lambda_s)}{K_d^{cyl}(\lambda_s)}\lambda_s^{-2}\right] \times \left(\frac{1}{D_s\mu}\right) \quad (28)$$

via λ_s. It is clear from Figure 18 that a temperature-dependent r_p alone is not capable of accounting for all of the experimental results. In order to do so, we must include the temperature dependence of the effective membrane thicknesses (level 3).

In Figure 18, we observe that the level 3 description does a very good job of accounting for the experimental rejections of the four solutes. As in level 2, the changes in r_p influence $\sigma_s(\lambda_s)$ and Pe_s, but now Pe_s is also influenced by the temperature-dependent ratio $l^{s}_{eff}/l^{w}_{p,eff}$

$$Pe_s \propto \left(\frac{l^{s}_{eff}}{l^{w}_{p,eff}}\right)\left[\frac{K_c^{cyl}(\lambda_s)}{K_d^{cyl}(\lambda_s)}\lambda_s^{-2}\right] \times \left(\frac{1}{D_s\mu}\right) \quad (29)$$

The changes in rejection as a function of T will thus depend intimately on how $l^{s}_{eff}/l^{w}_{p,eff}$, $[K_c^{cyl}(\lambda_s)/K_d^{cyl}(\lambda_s)]\lambda_s^{-2}$, and $\sigma_s(\lambda_s)$ change with temperature. In Figure 17b, we observe that $l^{s}_{eff}/l^{w}_{p,eff}$ decreases between 22 and 40 °C and then either increases (sucrose, glucose, glycerin) or remains roughly constant (arabinose)

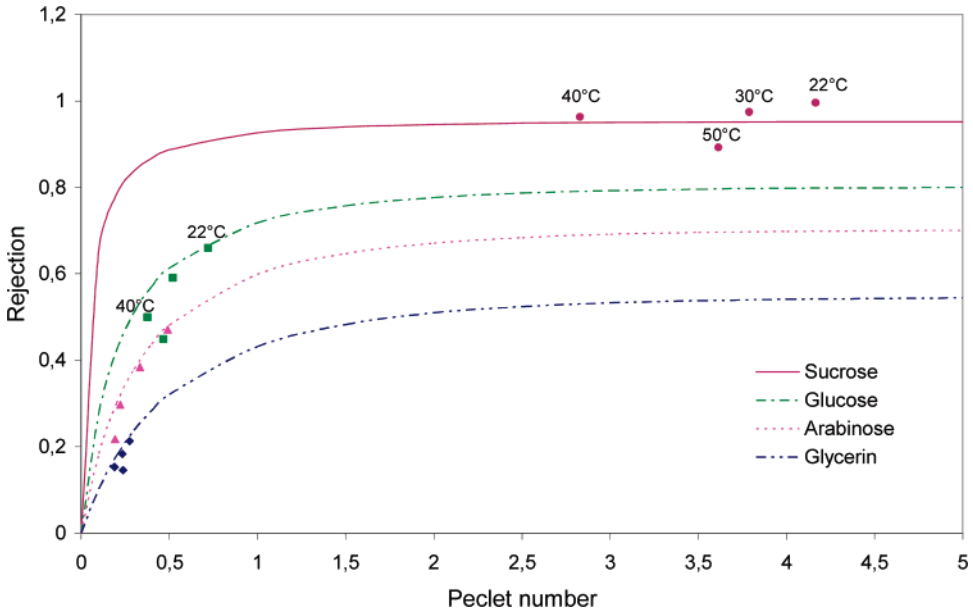

Figure 20. Rejection vs Peclet number at a fixed pressure of 13 bar (model curves and data for four solutes at four temperatures); the pore radius is taken to be the average of the three lowest (approximately equal) level 3 values (T = 22, 30, 40 °C).

between 40 and 50 °C. Because r_p increases with T, λ_s decreases, and therefore the importance of the second factor in eq 29, which has a flat minimum near $\lambda_s \approx 0.45$, will depend on the exact values taken on by λ_s (cf. Figure 19).

The observed and level 3 model rejections of sucrose, the largest solute, remain roughly constant between 22 and 40 °C and then drop at 50 °C. This is because the sucrose rejection between 22 and 40 °C is far into the high Péclet (flux) plateau at 13 bar and r_p increases only slowly (level 3, Figure 11 and Table 4). This is shown in Figure 20 where the rejection vs Péclet number (eq 8) is plotted for the four solutes using a fixed pore radius equal to the average over (the nearly equal) level 3 values for the three lowest temperatures. Thus, despite the large changes in Péclet number with temperature for sucrose (Figure 20), these have little or no effect on rejection. On the other hand, because the level 3 values for r_p abruptly increase when going from 40 to 50 °C, λ_s decreases, and the sucrose rejection follows suit.

The three smaller solute rejections are in the intermediate regime where both Pe_s and σ_s play significant roles (cf. eq 10). Because these three solutes (glucose, arabinose, glycerin) have λ_s values near the minimum of the curve in Figure 19, the second factor in Pe_s (eq 29) plays only a minor role. Therefore, the changes in Pe_s with T come predominantly from the temperature dependence of $l^s_{eff}/l^w_{p,eff}$, the first factor in eq 29. A glance at Figures 17b and 20 shows that this Péclet number effect is especially pronounced between 22 and 40 °C for these smaller solutes, as r_p is roughly constant (and therefore, σ_s varies little) in this temperature range. In going from 40 to 50 °C, the situation is now more complex for these three solutes, because the abrupt increase in r_p, which leads to a decrease in σ_s, is partially offset by an increase in Pe_s due the increase in the $l^s_{eff}/l^w_{p,eff}$ ratio (at least for glucose and glycerin, this ratio remaining roughly constant for arabinose in this temperature range). For glucose and arabinose, on one hand, the drop in σ_s due to the increase in r_p between 40 and 50 °C wins out over the increase (glucose) or lack of change (arabinose) in Pe_s, and the rejection drops substantially (Figures 18 and 20). On the other hand, for glycerin there is nearly exact compensation between these two competing effects, and the rejection hardly changes between 40 and 50 °C (Figures 18 and 20).

Conclusions

The answer to the question of whether or not the known bulk temperature dependences of μ and D_s are sufficient to account quantitatively for the temperature dependence of solute nanofiltration rejection is now clear: the bulk temperature dependences of μ and D_s can only explain a small (fixed flux) or negligible (fixed pressure) part of the decrease of solute rejection with increasing T. In order to account fully for the experimentally observed rejection drops obtained for the Desal5DK membrane within the framework of the HT model, we have been obliged to take into consideration the temperature dependence of both the effective membrane pore size and the solute-dependent effective thickness. In doing so, we have found that the HT model in its present form retains its ability to give very good simultaneous fits to experiment over a wide temperature range (22 to 50 °C) for as many as four different solutes, covering a wide range of solute-to-pore radius ratios: $\lambda_s = r_s/r_p = 0.39 - 0.81$. These results lend credence to the notion that it is possible to define a single, albeit temperature-dependent, effective pore size which is the same for all solutes.

The major features of the results presented here are as follows: (1) r_p is roughly constant (within statistical error) between 20 and 40 °C and then attains a statistically significant higher value (+15%) at 50 °C, an increase that we postulate to be correlated with temperature-dependent changes in the polymer membrane structure (thermal dilation); and (2) the effective membrane thickness is both solute size and temperature-dependent with at times non-monotonic variations as a function of both of these quantities (trends that need to be confirmed by further experiments with more lower-pressure data points, because the observed variations are near or beyond the limit of statistical significance within the framework of the analysis performed here). If we neglect all other except hindered transport (steric/hydrodynamic) interactions for polymer membranes, then neutral solute rejection evolves with increasing temperature as if the effective pore radius and effective thickness also evolve. On the basis of these results,

we have suggested that for these types of membranes one of the major effects explaining rejection drop with increasing temperature is thermal pore dilation; if so, then one might expect this effect to be absent in ceramic membranes, and a preliminary analysis of the rejection data appearing in ref 9 seems to show that this is indeed the case (a more firm conclusion must await completion of this work in progress[25]). Our tentative conclusions, awaiting possible corroboration by more detailed investigations, are that (1) temperature-dependent structural changes in polymer nanofilters play a significant role in the temperature dependence of neutral solute rejection via hindered transport effects and (2) secondary interactions do not play a major role in the rejection of rather large neutral solutes (at least those with not too large dipole moments), perhaps in part due to the canceling out of competing interactions.

The results presented in Figures 9, 10, 12, 14, and 18 show not only that the temperature dependence of r_p and l^s_{eff} must be taken into account in order for the HT model to describe the observed rejection changes as a function of temperature, but also that these changes result from a subtle interplay between the influences of σ_s and Pe_s (via the temperature dependence of r_p in the first case and r_p and l^s_{eff} in the second). This interplay is very likely the explanation for the at times conflicting results found in the literature concerning the temperature dependence of solute rejection. In order to get a better understanding of the types of temperature-dependent behavior that we have observed here, we intend to carry out partitioning and transport modeling studies at the nanoscale using approximate statistical mechanical methods, such as density functional theory, and molecular computer simulation methods.[21,26] We also intend to carry out further studies on single and multisolute mixtures (see refs 27 and 28 for UF studies) and on the temperature dependence of ion rejection by charged NF membranes. These studies can be considered a part of the growing industrially important field of solvent and solute transport in nanoporous media.[29−32]

Appendix 1: Diffusive and Convective Hindrance Factors

We present here approximate analytic expressions for the diffusive and convective hindrance factors appearing in the hindered transport (HT) model:[18]

$$K_d = \frac{6\pi}{K_t(\lambda)} \text{ and } K_c = \frac{(2-\Phi_s)K_s(\lambda)}{2K_t}$$

with

$$K_t(\lambda) = \frac{9}{4}\pi^2\sqrt{2}\,(1-\lambda)^{-5/2}\,[1+\sum_{n=1}^{2} a_n(1-\lambda)^n] + \sum_{n=0}^{4} a_{n+3}\lambda^n$$

and

$$K_s(\lambda) = \frac{9}{4}\pi^2\sqrt{2}\,(1-\lambda)^{-5/2}\,[1+\sum_{n=1}^{2} b_n(1-\lambda)^n] + \sum_{n=0}^{4} b_{n+3}\lambda^n$$

(26) Murad, S.; Oder, K.; Lin, J. *Mol. Phys.* **1998**, *95*, 401−408.
(27) Tam, C. M.; Tremblay, A.Y. *J. Membr. Sci.* **1990**, *57*, 271−287.
(28) Tweddle, T. A.; Striez, C.; Tam, C. M.; Hazlett, J. D. *Desalination* **1992**, *86*, 27−41.
(29) Martin, C. R.; Nishizawa, M.; Jirage, K.; Kang, M. *J. Phys. Chem. B* **2001**, *105*; 1925−1934.
(30) Chun, K.-Y.; Stroeve, P. *Langmuir* **2002**, *18*, 4653−4658.
(31) Liu, X.; Bruening, M. L. *Chem. Mater.* **2004**, *16*, 351−357.
(32) Liu, Y.; Wang, Q.; Linghong, L. *Langmuir* **2004**, *20*, 6921−6926.

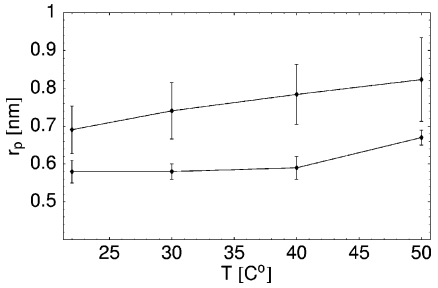

Figure A2.1. Fitted results and standard errors for the membrane pore radius as a function of temperature, obtained using the direct hindered transport theory method employed here (lower points) and using the combined Spiegler−Kedem/hindered transport theory method (upper points).

Table A2. 1. Fitted Pore Radius and Standard Error as a Function of Temperatures Using the Combined Spiegler−Kedem/Hindered Transport Theory Method

T (°C)	r_p (nm)	σ (nm)
22	0.69	0.06
30	0.74	0.07
40	0.78	0.08
50	0.82	0.11

where $a_1 = -73/60$, $a_2 = 77.293/50.4$, $a_3 = -22.5083$, $a_4 = -5.6117$, $a_5 = -0.3363$, $a_6 = -1.216$, $a_7 = 1.647$, $b_1 = 7/60$, $b_2 = -2.227/50.4$, $b_3 = 4.018$, $b_4 = -3.9788$, $b_5 = -1.9215$, $b_6 = 4.392$, and $b_7 = 5.006$.

Appendix 2: Model Fitting Procedure

We have used a χ^2 nonlinear fitting procedure (method of least squares) to fit the hindered transport theory to the experimental rejection vs volume flux density (j_v) data for the four neutral solutes (glycerin, arabinose, glucose, and sucrose) at a given temperature. For each data set, the model parameters that are adjusted to minimize the χ^2 merit function (sum of squared residuals) are a unique effective membrane pores size, r_p, common to all the solutes, and an effective membrane thickness for each of the four solutes (l^s_{eff}, s = glycerin, arabinose, glucose, and sucrose). We also perform a statistical analysis of the fitted values to estimate both the coefficient of determination, $R^2 \leq 1$, which is a gauge of the goodness of the overall fit, and the standard error (deviation), σ, associated with each of the five estimated model parameters. This is a nonstandard statistical problem, because one of the parameters, r_p, is shared among the four solutes. To the best of our knowledge, such a statistical analysis, based on applying the method of least squares to rejection vs volume flux density data, has not been previously performed in the field of NF. Other, most likely less reliable, methods have been used to estimate r_p and its associated standard error: In ref 20, for example, the Spiegler−Kedem form of the transport eq 4 is fit individually to each of the neutral solutes studied with P_s, the effective solute permeability, and σ_s, the solute filtration reflection coefficient, as fitting parameters. The effective membrane pore size is then estimated by a second least-squares fitting procedure, using various forms of hindered transport theory to calculate the solute filtration reflection coefficient (in ref 20, the form used here was not adopted, but rather an older Ferry model was used, along with some more recent variants). The data used in the fit are the previously fitted values of σ_s as a function of solute radius, r_s, and the model function fitted is the hindered transport theory prediction for limiting rejection, equal to the solute filtration reflection coefficient (which is a function

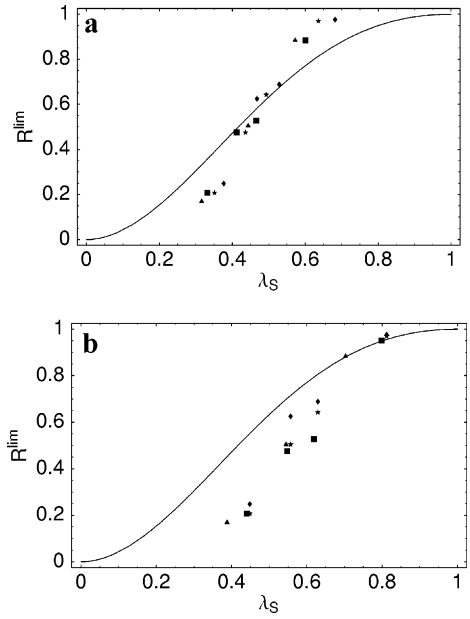

Figure A2.2. Theoretical hindered transport prediction (curve) and the estimated limiting rejection (from the first step Spiegler−Kedem fit to experiment), as function of the ratio $\lambda_s = r_s/r_p$ (a) using the combined Spiegler−Kedem/hindered transport theory values for r_p and (b) using the direct hindered transport theory values for r_p (method employed here).

of the ratio r_s/r_p). It is not clear what the total estimated error in r_p is for this double fitting procedure, because in ref 20, error estimates were only provided for the second fitting step (in passing, we note that no results were provided in this reference for the fitted values of P_s and associated errors).

In order to compare the two methods, we have analyzed our data as in ref 20 (combined Spiegler−Kedem/hindered transport method). With this last method, the value of σ_s is obtained by extrapolation to infinite flux; we therefore expect more accurate fits for the larger solutes, for which there are more points close to the limiting high flux plateau. The fitted results and standard errors for the membrane pore radius as a function of temperature, obtained using the Spiegler−Kedem/hindered transport method, are presented in Table A2.1 and plotted in Figure A2.1, along with the results obtained using our method. Although we observe the same trend of increasing pore radius with increasing temperature, the pore radii obtained using the Spiegler−Kedem method are consistently bigger (and possess much larger errors, even without incorporating the fitting errors coming from the first step Spiegler−Kedem fit, not shown in the figure). In Figure A2.2a, we plot the theoretical hindered transport curve (eq 13), along with the estimated limiting rejection (from the first step of the Spiegler−Kedem fit to experiment), as a function of the ratio $\lambda_s = r_s/r_p$ using the Spiegler−Kedem fitted values for r_p; in Figure A2.2b, we plot the same quantities, but now using the fitted values of r_p obtained using our method. (We do not plot the estimated limiting rejections obtained from our fitting procedure, because by construction they fall exactly on the theoretical hindered transport curve.) In the first figure, the largest discrepancies between theory and estimated limiting rejection are for small and large solutes, which is an artifact of the fitting method. In the second figure, the discrepancy between theory and estimated limiting rejection decreases with solute size, in line with what one would expect (because the values of σ_s coming from the first step Spiegler−Kedem fit are more accurate for the larger solutes). The ensemble of results obtained via the above comparison leads us to believe that the method we have adopted is more reliable than the two-step Spiegler−Kedem/hindered transport theory one.

Acknowledgment. We would like to thank the French Ministry of Foreign Affairs for partial funding (CMCU Project 04PRE01)

Glossary

c_m, c_p	membrane surface concentration, permeate concentration (M)
$\bar{c}$	mean solute concentration (M)
D_s	bulk solute diffusivity ($m^2\ s^{-1}$)
j_s	solute flux density (mol/(h m^2))
j_v^w, j_v	water, solution, volume flux density (L/(h m^2))
L_p^0	pure water permeability (L/(h m^2 bar))
l_{eff}^s	effective thickness of the membrane seen by the solute (μm)
$l_{p,eff}^w$	effective thickness of membrane seen by water evaluated from permeability (μm)
l_m	physical membrane thickness (μm)
Pe_s	Peclet number
P_s	effective solute permeability ($m^2\ s^{-1}$)
R	rejection coefficient
R_{lim}^i	highest rejection coefficient
r_i	solute radius (nm)
r_p	pore radius (nm)
T	temperature (°C)
K_c, K_d	hindered transport factors
ΔP	mean transmembrane pressure (bar)
$\Delta\pi$	osmotic pressure difference across the membrane (bar)
λ_s	ratio of solute to pore radius
τ_s	tortuosity factor
ϕ_p	porosity factor
Φ_s	solute partition coefficient
Φ_{steric}	solute steric partition coefficient
μ	dynamic water viscosity (Pa s)
σ_s	filtration reflection coefficient

LA060268P